

**High Resolution Mid-Infrared Imaging
of the Nucleus of NGC 1068**

J. J. Bock, K. A. Marsh, M. E. Ressler, and M. W. Werner
Jet Propulsion Laboratory, 4800 Oak Grove Drive, Pasadena, CA 91109

Received _____; accepted _____

Submitted to *Astrophysical Journal Letters* 1998 January 21

ABSTRACT

We have obtained mid-infrared images of the nucleus of NGC 1068 from the Hale 5 m telescope at Mt. Palomar with diffraction-limited resolution and high sensitivity at $\lambda = 8.8, 10.3, \text{ and } 12.5 \mu\text{m}$. Deconvolved images show that the infrared emission extends north to south in the inner $2''$, consisting of a central peak, a component extending $1''$ north of the central source, a component extending $1''$ south of the central source, and several smaller structures located $1''$ to the northeast. The central peak is extended $0.4''$ N-S and unresolved ($\leq 0.2''$) E-W. We find that $50 \pm 5\%$ of the flux emerges from the central $0.4''$ and that a single unresolved point source can account for only $27 \pm 5\%$ of the total flux. However, if the central peak arises from optically thick thermal emission, we estimate that the emitting region has a projected area $\geq 2 \text{ pc}^2$, and may thus contain a compact source such as a parsec-scale torus. The weak $10 \mu\text{m}$ silicate feature is observed to vary across the map, appearing most pronounced at the central peak. We observe a correspondence between the northern extension and the northeastern sources appearing on the mid-infrared images and the [OIII] clouds A - F. We interpret the faint optical counterpart to the mid-infrared southern extension as being due to partial obscuration by the intervening disk of the host galaxy. The N-S extension of the mid-infrared emission coincides with one wall of the conical narrow line region and aligns with the N-S orientation of the radio jet close to the nucleus. We interpret the infrared emission as arising from optically thick dust lining the walls of the low density cavity formed by the radio jet and heated by radiation from the central source.

Subject headings: galaxies: active, Seyfert — infrared: galaxies

1. Introduction

NGC 1068 represents the closest example of a Seyfert 2 galaxy ($D=14$ Mpc assuming $H_0 = 75 \text{ km s}^{-1} \text{ Mpc}^{-1}$, 68 pc/arcsec) and is thus amenable to study with high resolution imaging. A large bipolar radio jet (Wilson & Ulvestad 1987) originates near the active nucleus of the Sb(rs)II spiral host galaxy. The nucleus itself resolves into 4 distinct radio sources (Ulvestad, Neff, & Wilson 1987). High resolution optical imaging spectroscopy reveals that the narrow line region characteristic of Seyfert 2 galaxies has a roughly conical geometry (Evans et al. 1991; Macchetto et al. 1994) with complex gas motions (Arribas, Mediavilla, & Garcia-Lorenzo 1996). The morphologies of the narrow-line conical region and the radio jet are closely related (Gallimore, Baum, & O'Dea 1996b). The characteristic smooth optical continuum and very broad optical line emission associated with a Seyfert 1 galaxy can be seen in polarized light in NGC 1068 (Antonucci & Miller 1985), leading to the interpretation that NGC 1068 harbors an obscured Seyfert 1 nucleus. The absence of strong X-ray emission from the nucleus (Mulchaey, Mushotzky, & Weaver 1992) suggests that the nucleus is obscured by a column density of gas in excess of 10^{24} cm^{-2} .

The obscuring medium which prevents direct observation of the Seyfert 1 nucleus, but permits an indirect view in scattered polarized light, has an undetermined morphology. The obscuring medium may consist of a parsec-scale torus (see Antonucci 1993 and references therein) which would allow a direct view of the nucleus when viewed pole-on as in the case of a Seyfert 1 galaxy, but an obscured view when viewed edge-on as in the case of a Seyfert 2 galaxy such as NGC 1068. A torus geometry would also naturally explain the conical morphology of the narrow-line region observed in NGC 1068 and many other Seyfert galaxies (e.g. Mulchaey, Wilson, & Tsvetanov 1996). Recent observations provide indirect support for a compact torus. Interferometric observations of the rotational kinematics of water masers in the nucleus of NGC 1068 (Gallimore et al. 1996b; Greenhill et al. 1996)

indicate the presence of molecular material as close as 0.4 pc to the purported nucleus. Near-infrared speckle and adaptive optics imaging find that a compact ($< 0.03''$) source can account for 94% of the K-band emission in the central $1''$ (Thatte et al. 1997).

Mid-infrared observations of the nucleus of NGC 1068 (Braatz et al. 1993), however, show that the emission is dominated by a resolved component. If the mid-infrared emission is due to dust heated by radiation from a concealed Seyfert I nucleus, the bulk of the energy from the central source is actually intercepted not by a compact torus but by material located up to 100 pc away from the nucleus. Cameron et al. (1993) instead propose that the central source is obscured by a large envelope of clumpy molecular material known to surround the nucleus (Blietz et al. 1994; Planesas, Scoville, & Myers 1991), and that the mid-infrared emission originates from clouds in the molecular material exposed to radiation from the central source. The morphology of the material obscuring the nucleus of NGC 1068 is thus uncertain and may be more complex than a simple torus.

NGC 1068 emits strongly in the infrared, with the spectral energy distribution (SED) peaking at mid-infrared wavelengths (Roche et al. 1991). Mid-infrared imaging thus allows a relatively unobscured view with high spatial resolution of the emission process responsible for the bulk of the observed bolometric nuclear luminosity. Previous mid-infrared imaging (Braatz et al. 1993) detected the extended nature of the nuclear emission and determined that the emission arises from both an extended component and an unresolved central component. Our observations from the 5 m Hale telescope offer improved images with higher spatial resolution and sensitivity.

2. Observations

We conducted observations from the Cassegrain focus of the 5 m Hale telescope on Mt. Palomar on the nights of 1995 December 3-4 using MIRLIN, a new mid-infrared broadband camera developed at JPL (Ressler et al., 1994). MIRLIN is based on the HF-16 128×128 Si:As BIB array fabricated by Boeing (formerly Rockwell). The large well depth of 3×10^7 e^- /pixel makes the detector particularly well-suited for use under the large photon backgrounds encountered in broadband ground-based mid-infrared astronomy. Twin filter wheels allow the observer to select a wide array of filters, including a narrow-band CVF, for observations in the atmospheric windows in the spectral band $5 \mu\text{m} - 26 \mu\text{m}$. We selected 3 bands within the N-band atmospheric window with moderate spectral bandwidth ($\Delta\lambda/\lambda = 10\%$), centered at $\lambda = 8.8, 10.3,$ and $12.5 \mu\text{m}$, for our observations of NGC 1068. Although MIRLIN is somewhat more sensitive observing with a broadband N filter, we chose the narrower bands to probe the depth of the $10 \mu\text{m}$ dust silicate feature. We used a plate scale of $0.15'' \text{ pixel}^{-1}$ to obtain fully sampled images.

The target was observed in a standard "chop-nod" scheme to remove the foreground emission from the telescope and the atmosphere. We typically chopped at 1.25 Hz, coadding the 50 ms integrations at each mirror position to obtain on and off beam images A and B. After 20 s the telescope was nodded and the observation repeated to obtain 2 further images C and D. The observation cycle was repeated multiple times, dithering the position of the telescope several arc seconds after each cycle in order to sample different pixels on the detector. We obtained a single background-subtracted exposure by accurately registering each group of images $(A_i-B_i)-(C_i-D_i)$ using the bright nucleus of NGC 1068 and then coadding the multiple observations, $\Sigma_i [(A_i-B_i)-(C_i-D_i)]$.

We repeated the observation cycle several times for each of the three wavelength bands, observing NGC 1068 for a total of 2.5 hours on 3 December and 0.7 hours on 4 December.

The results reported in this paper are derived from the data obtained on 3 December with a small chop and nod throw (both 10") in order to keep the nucleus on the array at all times and to realize maximum sensitivity on the compact nucleus. Observations on 4 December were obtained with a 20" throw and confirmed that extended emission around the nucleus is sufficiently compact as to not appreciably alter the results obtained with the 10" throw.

3. Analysis

The images obtained in the chop-nod observations are registered and coadded to produce the raw images displayed with logarithmic contours in Fig. 1. The raw images of NGC 1068 represent a signal-to-noise ratio in total flux in excess of 10^3 , and a peak signal in excess of 10^2 times the per pixel noise level, where the noise is estimated from the off-source data. The images of the PSF calibrator α Tauri display the lobed diffraction pattern characteristic of the 5 m Hale telescope and have a signal-to-noise ratio in total flux greater than 10^4 . The raw images of NGC 1068, which have a spatial resolution FWHM = 0.5", clearly show that the nucleus is extended north to south in the inner regions.

EDITOR: PLACE FIGURE 1 HERE.

During the night of 3 December we observed, in sequential order over 2.5 hours, β Andromedae (AM = 1.1), NGC 1068 (1.6), β And (1.0), NGC 1068 (1.35), β And (1.0), and α Tauri (1.4). The multiple observations of β And serve to monitor any changes in the point spread function (PSF) due to atmospheric fluctuations or drifts in the focus of the telescope. Approximately one hour after observing NGC 1068 at transit, we observed α Tau at a nearly identical airmass. The measured flux of NGC 1068 and the reference stars are stable within each observation, showing < 5% fluctuations between exposures due to variations in atmospheric transparency. Unfortunately, the appreciable (20%) change in flux between the

two observations of NGC 1068 and the discrepancy in the cross-calibration of the reference stars indicate that weather conditions were not suitable for accurate photometry.

3.1. Deconvolution

The mid-infrared images are deconvolved using a technique developed by Richardson & Marsh (1983) (also see Marsh et al. 1995) which yields the most probable image based on the assumptions of Gaussian prior statistics with positivity in the pre-convolved image and measurement noise statistics described by a Gaussian with zero mean. We can obtain qualitatively similar results by instead deconvolving our images using a maximum likelihood routine.

The deconvolved image depends critically on the quality and stability of the PSF. Therefore, we frequently characterized the PSF between observations of NGC 1068, as described above, selecting calibration stars well-matched to the zenith angle of the target. Because α Tau is matched in air mass to NGC 1068 during the observations, we selected it for the point spread function in the deconvolution shown in Fig. 1. We can test the stability of the PSF during the observations by deconvolving the raw image of NGC 1068 using the PSF from β And instead of α Tau, obtaining similar results. We can also demonstrate the stability of the PSF by deconvolving the image of β And using the PSF from α Tau, resulting in a compact image with FWHM $\simeq 0.2''$ as shown in Fig. 1.

The deconvolved images of NGC 1068 show a central peak, and resolve structure elongated roughly north to south, in general accord with the deconvolved images reported by Braatz et al. (1993). The resolved emission in the deconvolved images of Braatz et al. (1993) is extended NE-SW with a deconvolved beam size of FWHM $\simeq 0.7''$. However, with higher angular resolution our data show that the resolved emission closer to the nucleus

actually extends N-S, as is evident in the raw images of NGC 1068 (FWHM = 0.5"). The flux of the central region, obtained by locating a 0.4" diameter false aperture on the peak, accounts for $50 \pm 5\%$ of the measured brightness in these images, consistent with the result of 54% from Braatz et al. (1993).

Resolved structures located to the northeast of the central peak are evident at each of the three wavelengths. Because these structures have low surface brightness, on order of 2% of the peak brightness, they are more sensitive to variations in the PSF. Nevertheless, the northeastern structures appear with a roughly hook-like geometry in all three wavelength bands, and are even evident in data (from other nights) rejected for poor atmospheric stability if deconvolved. Therefore we believe that the northeastern structures exist and are not an artifact of the deconvolution.

In our deconvolved images we find that the central peak, previously unresolved by Braatz et al. (1993), consists of a structure with width $\sim 0.2''$ (FWHM) E-W and width $\sim 0.4''$ (FWHM) N-S. Because the width in the E-W direction is similar to that of the deconvolved image of β And (0.2" FWHM), we consider the central peak to still be unresolved E-W. We can estimate the flux from the unresolved component by assuming that the deconvolved point spread function is a symmetric Gaussian with width equal to the E-W source width. If we assume that an unresolved point source is located at the peak, it accounts for $27 \pm 5\%$ of the total emission. The N-S extension of the central peak is better described, however, by an unresolved, uniform line source 0.4" in length. In this case this component accounts for $55 \pm 5\%$ of the total emission. Thus at least 73% of the total flux is resolved N-S in the deconvolved images.

If the mid-infrared peak contained a significant contribution from a point source which was partially obscured by dust, one might expect that the extracted point source would differ spectrally from the surrounding emission. However, the SED of the extracted

point source and the SED of the residual flux in the central $0.4''$ have silicate features with the same relative depth to within 10%. This is consistent with the large column density of obscuring material inferred from X-ray measurements blocking a direct view of the purported Seyfert I nucleus. We note that the near-infrared point source observed by Thatte et al. (1997), extrapolating to mid-infrared wavelengths, can account for only a small fraction (0.2 – 10%) of the total nuclear flux.

EDITOR: PLACE FIGURE 2 HERE.

In order to show the relative strength of the mid-infrared silicate feature, we plot the flux obtained in the deconvolved image in Fig. 2 over false apertures located on the central region, the northern extension, the southern extension, and the northeastern sources. Assuming the calibration obtained with α Tau, we note that the measured $F_{8.5\mu m} / F_{10.3\mu m}$ and $F_{8.5\mu m} / F_{12.5\mu m}$ flux ratios for the entire nucleus agree with Roche et al. (1991) to within 10%. The weak silicate feature is most pronounced in absorption at the central peak and is nearly absent over the extended regions.

3.2. Location of the Nucleus

Comparison of these mid-infrared images with high resolution radio and optical images aids in the interpretation of the data but requires an accurate registration between the maps. The narrow-line region (NLR), imaged in the $\lambda 5007 \text{ \AA}$ emission line of [OIII] with high spatial resolution using the corrected Hubble Space Telescope (Macchetto et al. 1994), shows clumpy emission in a roughly conical geometry. High resolution radio maps of the nucleus of NGC 1068 resolve 4 distinct sources and a collimated bipolar jet (Ulvestad et al. 1987). The position of the central source in NGC 1068 has been estimated by numerous authors, most notably by: 1) finding the center of UV polarization (Capetti et al. 1995);

2) registering the peak of the infrared emission with respect to the optical peak (Braatz et al. 1993; Thatte et al. 1997); and 3) locating the S1 radio source on the [OIII] image (Gallimore et al. 1996b; Capetti, Macchetto, & Lattanzi 1997b). The water masers located at the S1 radio source trace out a velocity gradient which can be described as an edge-on Keplerian disk associated with a compact torus obscuring the central source. Because we did not obtain accurate astrometry of the mid-infrared images, we place the peak of our deconvolved mid-infrared image at the location of the mid-infrared peak determined by Braatz et al. (1993).

In Fig. 3 we place the deconvolved $12.5 \mu\text{m}$ mid-infrared image over the [OIII] HST map, including the positions of the 4 radio sources. The [OIII] emission forms an extended, roughly conical region whereas the mid-infrared emission is concentrated in a compact region elongated north to south. The correspondence between the infrared northern extension with the [OIII] clouds A-C & E and between the infrared northeastern sources and the [OIII] clouds D & F suggests that the registration between the maps is indeed accurate. Given the limitations of the astrometry, we cannot discern if the northern extension coincides with the peaks of the [OIII] clouds A-C & E, or is displaced to the west by $\sim 0.15''$. The central peak and southern extension in the mid-infrared emission do not have distinct counterparts in the [OIII] map. The northern extension appears to trace the western wall, and the southern extension the eastern wall, of the conical narrow line region (Pogge 1989). With the exception of the weak northeastern sources, mid-infrared emission is largely absent from the conical region itself. A comparison between the mid-infrared emission and a 5 GHz map of the radio continuum (Gallimore et al. 1996b) (see Fig. 4), shows that the north-south extension of the mid-infrared emission aligns with the north-to-south orientation of the radio jet close to the nucleus.

EDITOR: PLACE FIGURE 4 HERE.

4. Discussion

The copious infrared nuclear emission of NGC 1068 ($L \sim 10^{11} L_{\odot}$), originates from thermal dust emission extending out to ~ 70 pc. The dust emission is associated with a gas mass of at least $M > m_H [F_{\nu}/B_{\nu}(T)] D^2 (10^{23} \text{ cm}^{-2}) = 10^4 M_{\odot}$. Several mechanisms have been proposed to heat the dust (radiation from a Seyfert I nucleus, star forming regions, shocks). Tresch-Fienberg et al. (1987) propose that the northeastern sources might arise from star formation. In addition to a lack of evidence for significant star formation near the nucleus (Cameron et al. 1993), we find that at higher resolution the northeastern sources contain only a small fraction ($\sim 10\%$) of the total flux. The nuclear stellar core observed in K-band imaging to extend out to $2.5''$ contributes a minority of the total nuclear luminosity unless the stars are very young ($< 10^7$ years old, Thatte et al. 1997). Capetti, Axon, & Macchetto (1997a) suggest that shocks may explain the ionization structure observed in optical line emission. Unfortunately, the location of these shock fronts are $4''$ from the nucleus and outside of the central region we image in the mid-infrared. Furthermore, shocks fail to provide sufficient energy to explain the observed mid-infrared flux in the central region (Cameron et al. 1993). Radiation from a Seyfert I nucleus alone is sufficient to supply the necessary luminosity and can heat dust out to large distances (Braatz et al. 1993).

The silicate feature shown in Fig. 2 appears weakly throughout the extended regions and is more pronounced at the nucleus. The lack of a strong silicate feature might be explained by depletion of silicate grains. However, if we ignore the silicate feature and compute the effective color temperature assuming optically thin dust emission, $I_{\nu} \propto \nu^1 B_{\nu}(T)$, where $B_{\nu}(T)$ is the blackbody function, we find T ranges from 220 K - 280 K over the central region and the northern and southern extensions (also see Tresch-Fienberg et al. 1987). Since this temperature is far below the expected sublimation temperature

Rotaciuc et al. 1991).

4.2. Southern Extension

The southern mid-infrared extension does not appear to have a clear optical NLR counterpart, although some structure is notable in the [OIII] map to the south of the nucleus. A modest quantity of dust in the intervening disk of the host galaxy may obscure the [OIII] emission from the southern cone, and indeed a clearer view of the southern counter-cone may be obtained in polarized near-infrared images (Packham et al. 1997). We note that the [OIII] to mid-infrared ratio is 5 times weaker along the southern extension than the northern extension, giving an obscuration of $A_V = 1.7$ if the northern extension and southern extension are under similar physical conditions. This estimate is in general agreement with the column density of gas, $N_H \sim 2 \times 10^{21} \text{ cm}^{-2}$, estimated by Macchetto et al. (1994) based on the reddening of the southern lobe. We note that asymmetry in the northern and southern brightness observed in the radio (see Fig. 4) also holds in the mid-infrared as the northern extension appears to be approximately twice as luminous as the southern extension.

4.3. Unresolved Component

We can estimate the projected area of the emission in the central region with a simple blackbody argument if the emission is optically thick, $A = D^2 F_\nu / B_\nu(T)$, where $D = 14$ Mpc is the distance to NGC 1068 and assuming $T = 350$ K. Including the entire flux from the central $0.4''$, which is well described by a line source, we find that the emitting area is 4 pc^2 . Assuming the flux obtained by removing a point source at the central peak (see section 3.1), the emitting area is 2 pc^2 . Thus the mid-infrared peak may harbor a compact source,

Rotaciuc et al. 1991).

4.2. Southern Extension

The southern mid-infrared extension does not appear to have a clear optical NLR counterpart, although some structure is notable in the [OIII] map to the south of the nucleus. A modest quantity of dust in the intervening disk of the host galaxy may obscure the [OIII] emission from the southern cone, and indeed a clearer view of the southern counter-cone may be obtained in polarized near-infrared images (Packham et al. 1997). We note that the [OIII] to mid-infrared ratio is 5 times weaker along the southern extension than the northern extension, giving an obscuration of $A_V = 1.7$ if the northern extension and southern extension are under similar physical conditions. This estimate is in general agreement with the column density of gas, $N_H \sim 2 \times 10^{21} \text{ cm}^{-2}$, estimated by Macchetto et al. (1994) based on the reddening of the southern lobe. We note that asymmetry in the northern and southern brightness observed in the radio (see Fig. 4) also holds in the mid-infrared as the northern extension appears to be approximately twice as luminous as the southern extension.

4.3. Unresolved Component

We can estimate the projected area of the emission in the central region with a simple blackbody argument if the emission is optically thick, $A = D^2 F_\nu / B_\nu(T)$, where $D = 14$ Mpc is the distance to NGC 1068 and assuming $T = 350$ K. Including the entire flux from the central $0.4''$, which is well described by a line source, we find that the emitting area is 4 pc^2 . Assuming the flux obtained by removing a point source at the central peak (see section 3.1), the emitting area is 2 pc^2 . Thus the mid-infrared peak may harbor a compact source,

such as a parsec-scale dusty torus. If the emission is obscured by intervening dust or is optically thin however, the source size will be underestimated (although the weakness of the silicate feature and small variation in the color temperature over the central region suggests that these effects are small). If the central source consists of emission from regions of dust at several different temperatures, partially obscured by cooler dust (Heisler, Lumsden, & Bailey 1997), the spectrum and effective size of the central source are model dependent.

4.4. Morphology

If the mid-infrared emission is indeed powered by radiation from the central source, then the morphology of the mid-infrared emission denotes regions where radiation from the central source is absorbed by dust and converted to thermal infrared radiation. Some of the energy actually may be reradiated first by hot ($T \sim 1000K$) dust close to the central source. However, the relatively low inferred bolometric luminosity of the K-band point source observed by Thatte et al. (1997) in NGC 1068 and the lack of prominent near-infrared emission in the SED's of Seyfert I and II galaxies (Roche et al. 1991; Mas-Hesse et al. 1995) suggest that the fraction of reradiated energy is small.

We find that approximately half of the mid-infrared emission resides in the northern and southern extensions, reaching ~ 70 pc from the nucleus. Emission within the central $0.4''$ is partially resolved and extends ~ 15 pc north-to-south, leaving only $27 \pm 5\%$ of the total emission to reside in a central point source. Although a compact, unresolved point source may be located at the peak of the mid-infrared brightness, and evidence for a compact torus exists (Gallimore et al. 1996a; Greenhill et al. 1996), these data indicate that of the majority of the radiation from the central source (not including the fraction which escapes completely) is actually absorbed at distances greater than 10 pc. Therefore lines of sight to the nucleus must exist which are intercepted not by a compact torus but

by dust located far from the nucleus.

As an alternative to a simple torus, we suggest that the morphology of the obscuring medium, as traced by the mid-infrared emission, is related to the morphology of the radio jets. We observe that the mid-infrared emission in the central $0.4''$ is elongated N-S following the N-S orientation of the radio jet closest to the nucleus. This suggests that the mid-infrared emission arises from clouds lining the walls of a low density cavity heated by radiation from the central source. The walls of the low density cavity may be an extension of the compact structure mapped in H_2O maser emission with an opening angle of $\sim 90^\circ$ (Greenhill et al. 1996). The resolution of these deconvolved mid-infrared images is insufficient to distinguish if the emission in the central $0.4''$ has a linear or conical shape. A compact torus may be responsible for preventing radiation propagating E-W, explaining the N-S morphology of the mid-infrared emission.

Further from the nucleus, the northern and southern extensions of the mid-infrared emission align along a single wall of the conical ionization region. Although we can determine that the filling factor of the extensions is low, the data are insufficient to distinguish whether the emission consists of a coherent linear structure extending N-S to the nucleus which is unresolved E-W, or if it breaks up into small unresolved clumps. We note that mid-infrared and [OIII] emission are absent at the northernmost radio source NE, as would be expected if the radio jet has swept out a cavity of ionized gas (Capetti et al. 1997b; Gallimore et al. 1996b). We also observe that the northern extension terminates approximately at the location where the radio jet bends eastward, near the radio component C where the radio jet may be diverted by a giant molecular cloud (Gallimore et al. 1996b).

5. Conclusions

These images resolve the majority of the mid-infrared emission in the nucleus of NGC 1068 and show that emission from a compact central source can only account for a fraction of the total flux. With improved spatial resolution we determine that the resolved structure extends north-south in the innermost regions, corresponding to the orientation of the radio jet, with separate structures located to the northeast of the central source. We interpret the mid-infrared emission as arising from optically thick dust, extending out to ~ 70 pc, associated with a gas mass $M \geq 10^4 M_{\odot}$, and heated by radiation from the central Seyfert I nucleus. In order to explain the observed mid-infrared morphology we postulate that dust lines the walls of a low-density cavity, heated by radiation from the central source.

The work described in this paper was carried out at the Jet Propulsion Laboratory, California Institute of Technology, under an agreement with the National Aeronautics and Space Administration. We acknowledge the support of the JPL Director's Discretionary Fund and of NASA's Office of Space Science. Observations at the Palomar Observatory were made as part of a continuing collaborative agreement between Palomar Observatory and JPL. The authors thank the staff at Mt. Palomar for their assistance during the observations, J. F. Gallimore for providing the [OIII] and radio images, and David Seib for providing the focal plane array.

REFERENCES

- Antonucci, R. R. J. 1993, *ARA&A*, 31, 473
- Antonucci, R. R. J., & Miller, J. S. 1985, *ApJ*, 297, 621
- Arribas, S., Mediavilla, E., & García-Lorenzo, B. 1996, *ApJ*, 463, 509
- Blietz, M., Cameron, M., Drapatz, S., Genzel, R., Krabbe, A., Van der Werf, P., Strenberg, A., & Ward, M. 1994, *ApJ*, 421, 92
- Braatz, J. A., Wilson, A. S., Gezari, D. Y., Varosi, F., & Beichman, C. A. 1993, *ApJ*, 409, L5
- Cameron, M., Storey, J. W., Rotaciuc, V., Genzel, R., Verstraete, L., Drapatz, S., Siebenmorgen, R., & Lee, T. J. 1993, *ApJ*, 419, 136
- Capetti, A., Macchetto, F., Axon, D. J., Sparks, W. B., & Boksenberg, A. 1995, *ApJ*, 452, L87
- Capetti, A., Axon, D. J., & Macchetto, F. D. 1997a, *ApJ*, 487, 560
- Capetti, A., Macchetto, F. D., & Lattanzi, M. G. 1997b, *ApJ*, 476, L67
- Evans, I. N., Ford, H. C., Kinney, A. L., Antonucci, R. R. J., Armus, L., & Caganoff, S. 1991, *ApJ*, 369, L27
- Gallimore, J. F., Baum, S. A., O'Dea, C. P., Brinks, E., & Pedlar, A. 1996a, *ApJ*, 462, 740
- Gallimore, J. F., Baum, S. A., & O'Dea, C. P. 1996b, *ApJ*, 464, 198
- Greenhill, L. J., Gwinn, C. R., Antonucci, R., & Barvainis, R. 1996, *ApJ*, 472, L21
- Heisler, C. A., Lumsden, S. L., & Bailey, J. A. 1997, *Nature*, 385, 700

- Laor, A., & Draine, B. T. 1993, *ApJ*, 402, 441
- Macchetto, F., Capetti, A., Sparks, W. B., Axon, D. J., & Boksenberg, A. 1994, *ApJ*, 435, L15
- Marsh, K. A., Van Cleve, J. E., Mahoney, M. J., Hayward, T. L., & Houck, J. R. 1995, *ApJ*, 451, 777
- Mas-Hesse, J. M., Rodriguez-Pascual, P. M., de Cordoba, L. S. F., Mirabel, I. F., Wamsteker, W., Makino, F., & Otani, C. 1995, *A&A*, 298, 22
- Mathis, J. S. 1990, *ARA&A*, 28, 37
- Mulchaey, J. S., Mushotzky, R. F., & Weaver, K. A. 1992, *ApJ*, 390, 69
- Mulchaey, J. S., Wilson, A. S., & Tsvetanov, Z. 1996, *ApJ*, 467, 197
- Muxlow, T. W. B., Pedlar, A., Holloway, A. J., Gallimore, J. F., & Antonucci, R. R. J. 1996, *MNRAS*, 278, 854
- Netzer, H. 1990, in *Saas-Fée Advanced Course, Active Galactic Nuclei*, Vol. 20, ed. T. J. L. Courvoisier & M. Mayor (Berlin:Springer), 57
- Packham, C., Young, S., Hough, J. H., Axon, D. J., & Bailey, J. A. 1997, *MNRAS*, 288, 375
- Planesas, P., Scoville, N., & Myers, S. T. 1991, *ApJ*, 369, 364
- Pogge, R. 1989, *ApJ*, 345, 730
- Ressler, M. E., Werner, M. W., Van Cleve, J., & Chou, H. A. 1994, in *Infrared Astronomy with Arrays: The Next Generation*, ed. I. S. McLean (Dordrecht:Kluwer), 429
- Richardson, J. M., & Marsh, K. A. 1983, *Proc. SPIE*, 413, 79
- Roche, P. F., Aitken, D. K., Smiyh, C. H., & Ward, M. J. 1991, *MNRAS*, 248, 606

Rotaciuc, V., Krabbe, A., Cameron, M., Drapatz, S., Genzel, R., Sternberg, A., & Storey, J. W. V. 1991, *ApJ*, 370, L23

Thatte, N., Quirrenbach, A., Genzel, R., Maiolino, R., & Tecza, M. 1997, *ApJ*, 490, 238

Tresch-Fienberg, R., Fazio, G. G., Gezari, D. Y., Hoffman, W. F., Lamb, G. M., Shu, P. K., & McCreight, C. R. 1987, *ApJ*, 312, 5421

Ulvestad, J. S., Neff, S. G., & Wilson, A. S. 1987, *AJ*, 93, 22

Wilson, A. S., & Ulvestad, J. S. 1987, *ApJ*, 319, 105

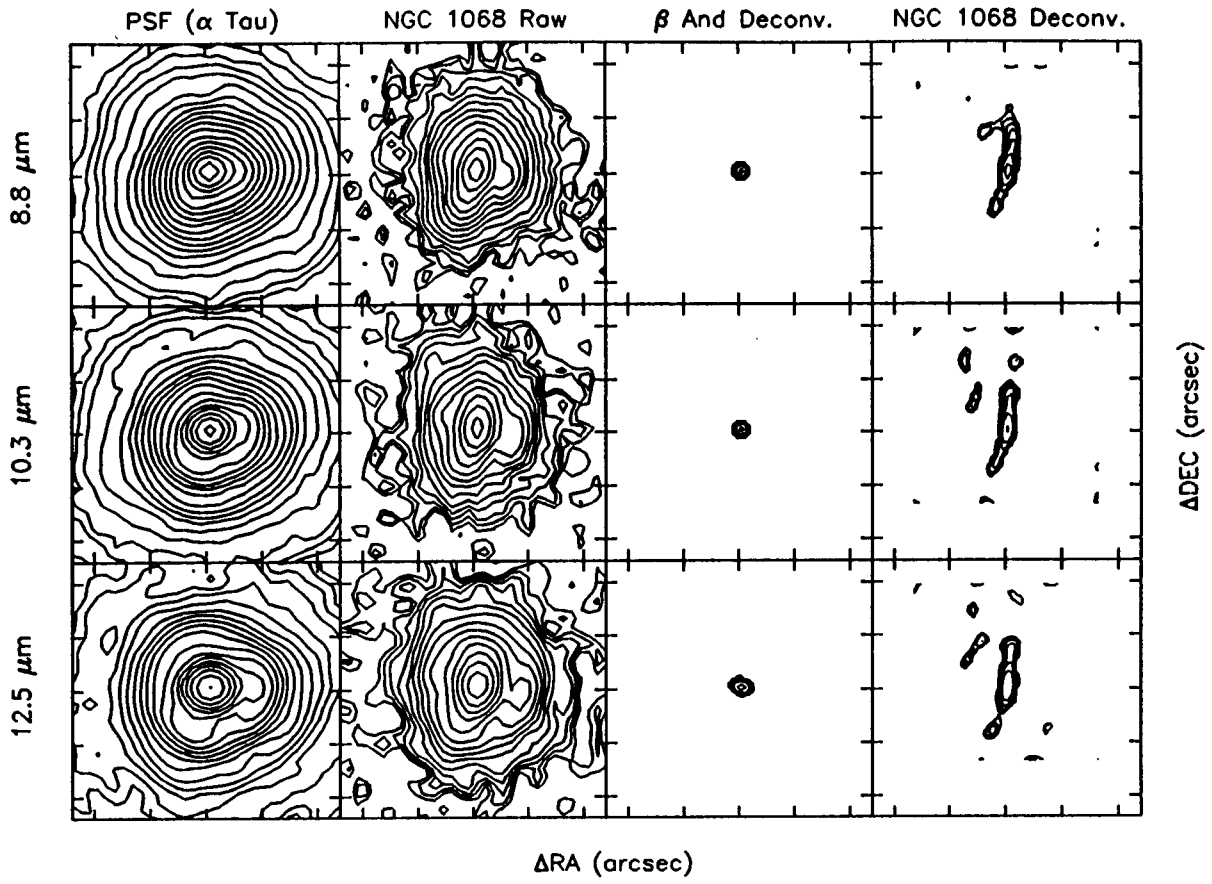
Fig. 1.— Panels from left to right show the point spread function derived from observations of α Tau, the raw image of NGC 1068, the deconvolved image of β And using the PSF from α Tau, and the deconvolved image of NGC 1068 using the PSF from α Tau. Wavelength bands of observation are $8.8 \mu\text{m}$ (top), $10.3 \mu\text{m}$ (middle), and $12.5 \mu\text{m}$ (bottom). For the raw images, contours begin at the 1σ level pixel^{-1} and increase by multiplicative factors of $\sqrt{2}$. The deconvolved images have 8 contours beginning at 0.8 of the peak value and decreasing by multiplicative factors of 2. The field of view in each panel is $4.8'' \times 4.8''$.

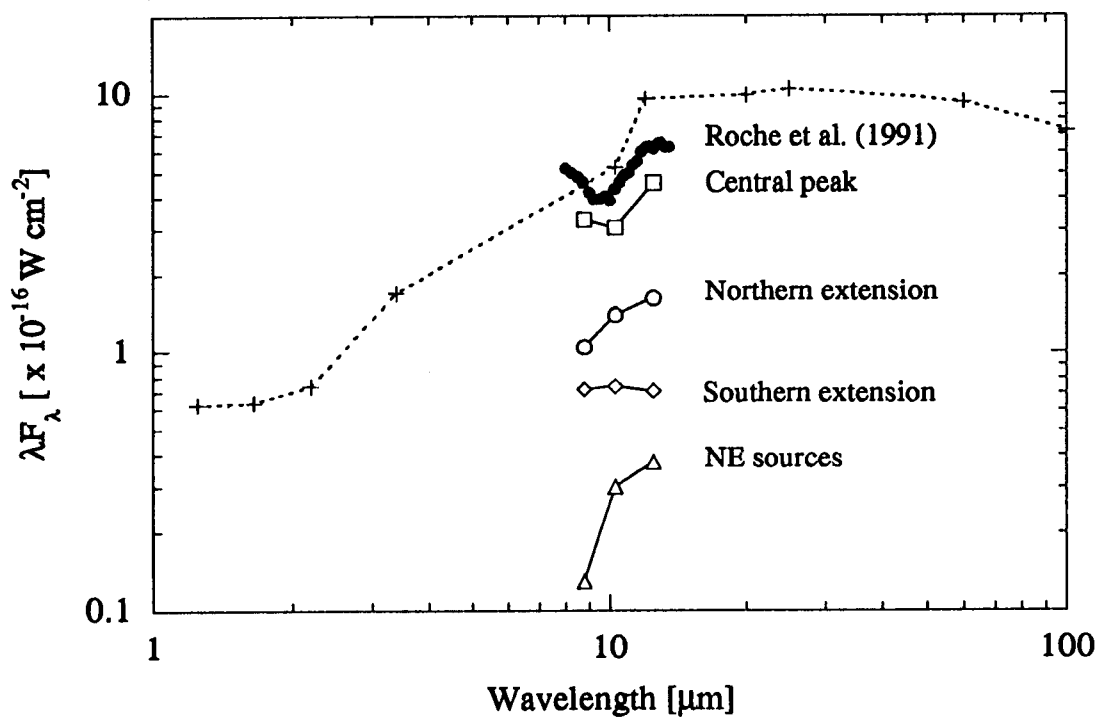
Fig. 2.— The spectral energy distribution of NGC 1068 (Roche et al. 1991, with $5''$ apertures from ground-based measurements and IRAS fluxes at 12, 25, 60 and $100 \mu\text{m}$) is shown with crosses and filled circles. Fluxes measured at 8.5, 10.3, and $12.5 \mu\text{m}$ indicate the varying depth of the weak silicate feature at the nucleus ($0.4''$ false aperture), the northern and southern extensions ($0.6''$ false apertures), and the northeastern sources ($1.5''$ false aperture).

Fig. 3.— Comparison of the deconvolved $12.5 \mu\text{m}$ image with the [OIII] $\lambda 5007 \text{ \AA}$ map of Macchetto et al. (1994). The contour spacing for the mid-infrared image is as in Fig. 1, and the [OIII] map is displayed with a logarithmic stretch. The letters label local maxima in the [OIII] emission as described by Evans et al. (1991). The green circle denotes the location of the mid-infrared peak determined by Braatz et al. (1993), the square denotes the location of the center of UV polarization (determined most recently by Capetti et al. 1997b), and the cross denotes the location of the near-IR peak determined by Thatte et al. (1997). Blue X's denote the location of the 4 radio peaks (S2, S1, C and NE from south to north) assuming the registration of Gallimore et al. (1996b). The size of each green symbol is equal to the positional uncertainty quoted by the authors.

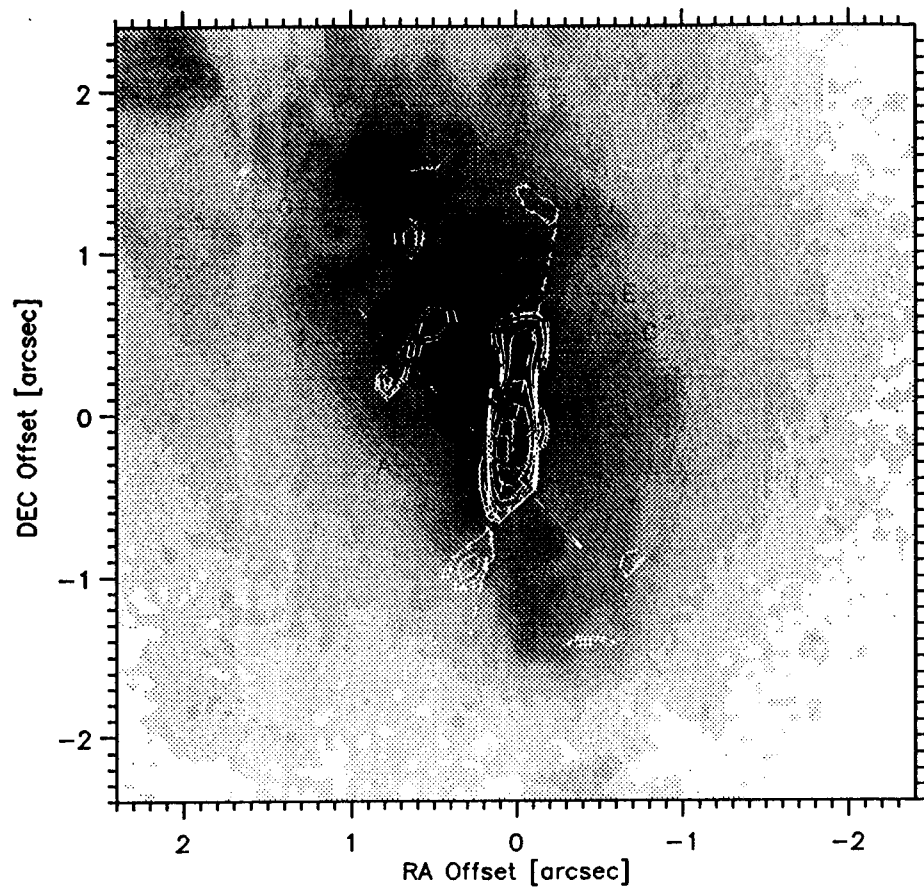
Fig. 4.— Comparison of the deconvolved $12.5 \mu\text{m}$ image with the 5 GHz map of Gallimore et al. (1996b). We register the maps by simply aligning the mid-infrared peak with S1,

consistent to within the error in registering the two images to the [OIII] map.





Comparison of [OIII] and IR Images



Comparison of Radio and IR Images

